

Automatic Extraction and Evaluation of Geological Linear Features from Digital Remote Sensing Data Using a Hough Transform

Amnon Karnieli, Amnon Meisels, Leonid Fisher, and Yaacov Arkin

Abstract

The Hough transform is an established tool for discovering linear features in images. The present investigation presents a new and specific algorithm for detecting geological lineaments in satellite images and scanned aerial photographs which incorporates the Hough transform, a new kind of a "directional detector," and a special counting mechanism for detecting peaks in the Hough plane.

Three test sites representing different geological environments and remote sensing altitudes were selected. The first site represents sedimentary conditions of chalk beds on cherry picker photography; the second represents plutonic conditions of granite rocks on an aerial photograph; and the third represents tectonic fractures of carbonates, chalks, and cherts on digital satellite data. In all cases, automatic extraction and mapping of lineaments conformed well to interpretation of lineaments by human performance.

Introduction

Regional study of linear features such as faults, joints, folds, dikes, crustal fracturing, and lithological contacts, using aerial photographs and particular satellite images, has made important advances in geological research during the last few decades (Rowan and Lathram, 1980). Recognition of lineaments has been used for investigating active fault patterns in areas of difficult accessibility (Tibaldi and Ferrari, 1991), water resources investigations (Waters, 1990), mineral deposit exploration (Rowan and Lathram, 1980), and in the study of the structural or tectonic history of a region.

The use of computerized, scanned data analysis for the detection of linear features from aerial photographs or digital satellite images can reduce to a minimum the bias of the subjective decision of the interpreter. Sijmons (1987) distinguished between two categories of computerized lineament processing. The first involves mainly enhancement of linear features using standard image processing methods (such as edge detection directional filters) for later visual interpretation while the second category involves automatic computer processing of the original digital data for the production of a lineament map. Obviously, the majority of studies which have been done up to date belong to the first category. For all of the cases in this category, interpretation of lineaments is still subjective, and considerable experience is required to detect weak features or to separate close ones. In order to overcome these limitations, an automatic objective procedure

is required. This type of procedure is not common (Oakes, 1987; Simon *et al.*, 1989; Zlatopolsky, 1992). During the last few years, special interest has been shown in using the Hough transform algorithm for this purpose, but with limited success (Cross, 1988; Cross and Wadge, 1988; Wang and Howarth, 1989; Wang and Howarth, 1990).

The approach in this study was to use the Hough transform in a special version that is more sensitive to grey level continuity in digital aerial photographs and satellite images. After the detection of strong linear features on the image, we examined the data available at different scales from a level of ground information compared to that obtained from aerial photographs and satellite data. The lineament data studied comes from a range of fracture patterns from a simple two-set pattern to a more complex one having three or more sets.

The Hough Transform Algorithm

The Hough transform is designed to detect collinear sets of edge pixels in an image by mapping these pixels into a parameter space (the Hough space) defined in such a way that collinear sets of pixels in the image give rise to peaks in the Hough space (Ballard and Brown, 1982). The edge pixels processed by the transform include the digital approximations of the gray level gradient magnitude m and direction θ .

A straight line can be characterized by its slope α and its perpendicular distance ρ from the origin. For the line with slope α that passes through the point (x, y) , we have

$$\rho = x \sin \alpha - y \cos \alpha. \quad (1)$$

Note that ρ is a signed quantity: e.g., if α is in the fourth quadrant and (x, y) is in the first quadrant, ρ is negative.

Suppose an image contains a long straight edge e having slope α and distance ρ from the origin. Then an edge pixel having coordinates (x, y) and lying on e should have gradient direction θ perpendicular to α , i.e., $\alpha = \theta \pm \pi/2$. Thus, in terms of θ , Equation 1 becomes

$$\begin{aligned} \rho &= x \sin (\theta \pm \pi/2) - y \cos (\theta \pm \pi/2) \\ &= \pm (x \cos \theta + y \sin \theta). \end{aligned} \quad (2)$$

If we compute ρ for each edge pixel using Equation 1, e should give rise to a cluster of (ρ, θ) values. Note that one needs compute only one ρ for each θ , depending on whether the positive gradient direction is $\theta + \pi/2$ or $\theta - \pi/2$.

Unfortunately, in practice one does not obtain "tight"

A. Karnieli, A. Meisels, and L. Fisher are with The Jacob Blaustein Institute for Desert Research, Sede Boker Campus, Ben-Gurion University of the Negev 84990, Israel.

Y. Arkin is with the Geological Survey of Israel, 30 Malkhe Yisrael St., 95501 Jerusalem, Israel.

Photogrammetric Engineering & Remote Sensing,
Vol. 62, No. 5, May 1996, pp. 525-531.

0099-1112/96/6205-525\$3.00/0

© 1996 American Society for Photogrammetry
and Remote Sensing

clusters from the edge pixels in a real image, because the gradient direction θ is difficult to compute accurately (Rosenfeld *et al.*, 1986). We will introduce, in the next section, a new method for computing directions of line segments that proves to be very useful for Hough transforming geological lineaments. This new method stands in clear contrast to the traditional method of obtaining the magnitude and direction of the gradient on small neighborhood operators. The overall inexactness of the direction of the gradient (based on small neighborhoods) induces a necessity to use a range of θ instead of one exact value when searching for clusters in the Hough plane (Rosenfeld *et al.*, 1986). Our approach leads to the intuitively correct state in which, if an image contains a long straight edge, it is possible to detect a cluster where all arcs (in the ρ, θ plane) that correspond to a given x, y and a range of θ intersect.

Let the input image be an $n \times n$ matrix; then the range of possible ρ values (in pixel units) is $n\sqrt{2}$, i.e., on the order of n . The number of distinct digitized straight lines through a given point in an $n \times n$ image is also on the order of n , i.e., there are only $\sim O(n)$ different slopes for these lines. Thus, when working with an $n \times n$ input image, we can use a digital (ρ, θ) space of size of the order of $n \times n$. We shall assume that the (ρ, θ) space is in fact an array of the same size as the image. The process of computing the Hough transform in the standard way is as follows:

- For each pixel (x, y) in the image, compute the edge magnitude $m = m(x, y)$ and its direction $\theta = \theta(x, y)$. Call (x, y) an edge pixel if $m(x, y) \geq T$, where T is a threshold.
- For each edge pixel (x, y) and each $\theta(x, y)$, compute $\rho = x \cos \theta + y \sin \theta$ and add 1 to the Hough array in position (ρ, θ) . Thus, in the final Hough array, the value at (ρ, θ) is the number of times the pair (ρ, θ) is obtained by processing all edge pixels in this way.

A Hough Algorithm for Geological Lineament Detection

Most reports of Hough transform extraction of linear elements from images use some simple edge detector for the measurement of gradient magnitude and direction (Ballard and Brown, 1982; Rosenfeld *et al.*, 1986). The basic image used in the present study to develop the algorithm is given in Figure 1. The use of a simple edge finder such as the Sobel operator generates a great amount of noise, resulting in the masking of geological lineaments (Figure 2). Consequently, it was necessary to develop an approach that produces a direction per pixel by searching a large neighborhood instead of calculating a gradient direction from a noisy 3 by 3 derivative.

This approach for extraction of edge directions complements the commonly used calculation of derivatives in that it searches over a large neighborhood for pixels which are similar to the central pixel. This operation is equivalent to identifying an edge, or line, by running along it rather than by crossing it (with an edge detector). The algorithm sums the differences in grey level along lines passing through the pixel in all possible directions. Whenever the sum of differences is smaller than a given threshold, the direction is considered "detected," in a way similar to the detection of a direction of a strong enough edge. For a neighborhood that includes a possible straight line of length n , grey level of a pixel i denoted by g_i , and the grey level of the central pixel denoted by g_0 , the thresholding test for extracting a line is performed by the use of the expression

$$\sum_{i=1}^n |g_i - g_0| \leq \text{Threshold.} \quad (3)$$

This detection approach is effective for lines that have one dark side and one bright side; otherwise, a homogeneous patch will trigger the threshold of Equation 3. However, our



Figure 1. Aerial photograph of Santa Katharina.

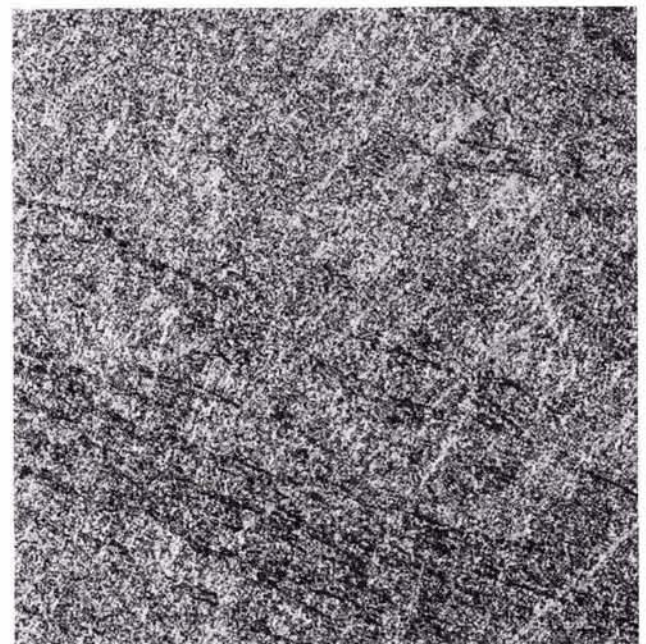


Figure 2. Results of edge detection on the Santa Katharina aerial photograph using the Sobel operator.

method is immune to this effect because we detect dark lines and bright lines separately and then merge them, as is described below.

In order to compare the general behavior of the directional filter of Equation 3 and a common edge detector, we present typical results in Figures 2 and 3. When applying our method of Equation 3, we used sizes of neighborhoods up to 20 by 20 pixels and an angular resolution in the direc-



Figure 3. The proposed directional search (on 20 by 20 neighborhoods) on the Santa Katharina aerial photograph.

tion of pixels of 5° . These are very large neighborhoods, compared to common 3 by 3 edge detectors. As a result, the detected directions are much more accurate than in the standard small edge detector case. Figure 2 presents the result of running the Sobel operator on Figure 1 with no threshold. Figure 3 presents the result of calculating the LHS of Equation 3, again with no thresholding. In both figures, brighter pixels have stronger directionality. The strength of our proposed mechanism of directional filtering is demonstrated by the fact that the darker pixels reside on visible lineaments in Figure 3 (bottom).

The next step in the Hough algorithm for line detection is to accumulate "counts" in the Hough plane, counts that represent candidate straight lines, and to look for peaks of these counts over the plane. The accuracy of the detected directions gives us reasons to expect that the process of counting votes for lines can be simplified by counting each pixel only once. Each pixel votes in the Hough plane for the line that passes through it and has the right direction. To improve the "shallowness" of the count space, we have applied a new form that is specifically suitable for detecting black-white lines. Instead of counting *pixels* on a thresholded line, our proposed algorithm counts *grey levels* for each candidate line point.

The proposed algorithm looks for lines of either dark shade or bright shade and takes care to merge the two complementary results. Counting grey levels produces a need to run the algorithm twice (on a picture and its inverse) to find all outstanding geological lineaments. However, it turns out that counting occurrences of lines in the Hough plane is much less sensitive to noise when one uses the above form of counts of line occurrence. In general, we adopt the common technique of denoting straight lines by a_{pa} (lines of slope α and distance ρ). As a result, we define the count of a line to be the following:

$$a_{pa} = \sum x_j \quad (4)$$

where x_j are the grey level values along the line a_{pa} , in the Hough plane.

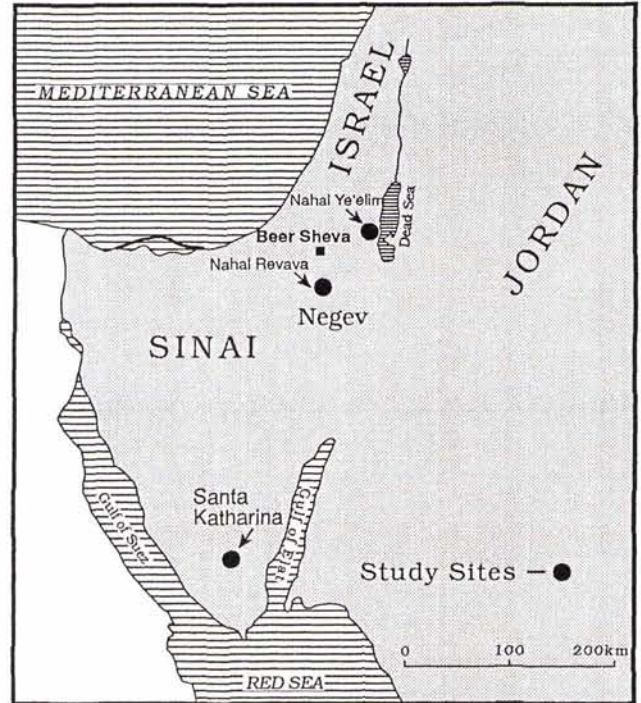


Figure 4. Location map.

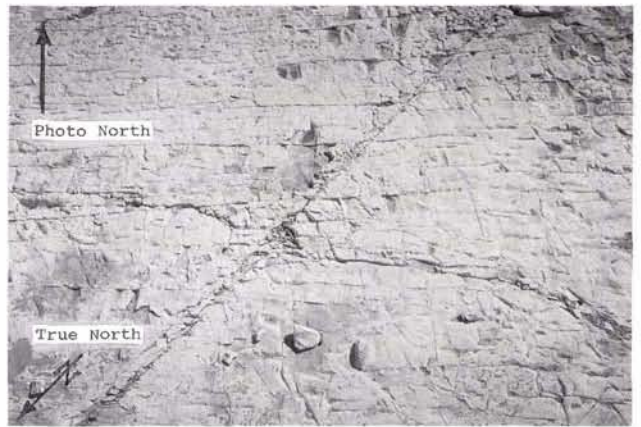


Figure 5. Nahal Revava outcrops of Eocene chalk.

The normalization of the counts in the Hough plane is performed by representing the count at each point a_{pa} as a relative value

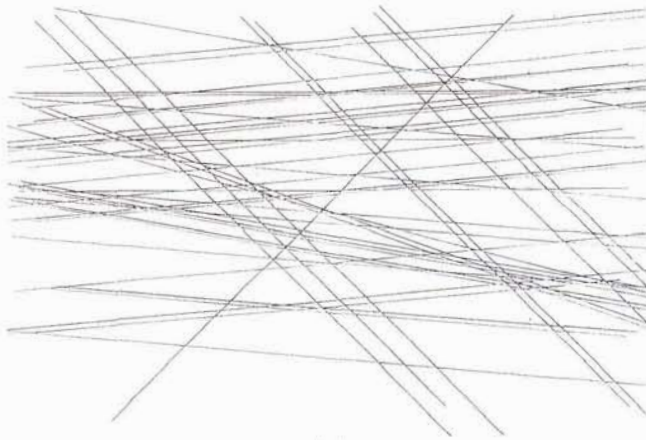
$$z_{pa} = \frac{a_{pa} - a_{\min}}{a_{\max} - a_{\min}} \quad (5)$$

where a_{\min} is the minimal value of the sum in Equation 4 for the Hough plane and a_{\max} is the corresponding maximal value. Our algorithm for detection of peaks in the Hough plane cuts off counts that have a value $z_{pa} \leq 0.7$. The two separate Hough planes, one for dark lines and one for bright lines, are thresholded separately.

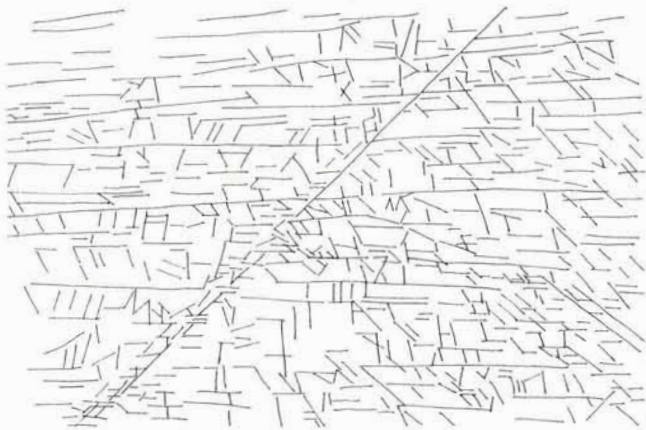
The final step in detecting the geological lineaments is in merging the lines that resulted from the peak detection in the Hough plane. Here, one has to merge similar lines, that



Figure 6. The Nahal Revaha test site.



(a)



(b)

Figure 7. Lineaments in the Nahal Revaha test site. (a) Automatic extraction. (b) Photograph interpretation.

is, lines that lie close enough to one another and in similar enough inclination. In the process of merging lines, one has to mix the populations of dark and bright lines, because real linear structures (and in photographs taken in non-zenith situations) generate strong linear responses in the analyzed pic-

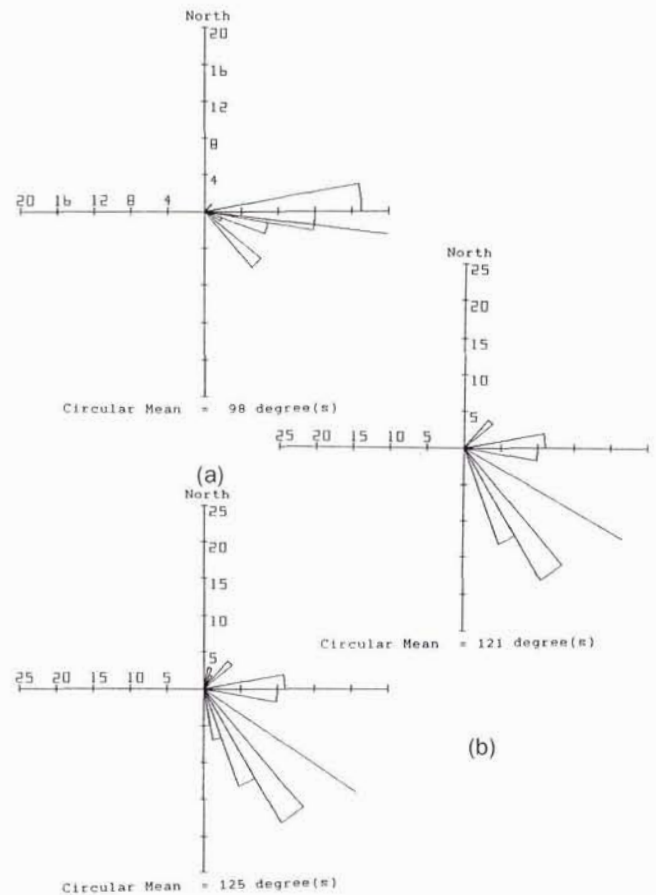


Figure 8. Rose diagrams for Nahal Revaha test site. (a) Automatic extraction. (b) Photointerpretation of main lineaments. (c) Photointerpretation of total lineaments.

ture of both dark and bright Hough peaks. In the present detection process, lines that are closer to one another than their own length, and that have the same inclination, were merged. Merging took place between pairs of lines of both similar and different shades. The final results of the above procedure will be presented and compared to those of the human interpreter in the following sections.

Application of Algorithm

In order to test the automatic extraction of geological linear features from digital remote sensing, it was necessary to obtain ground truth from test sites of known geological features which could be verified by mapping or from previously published data. Furthermore, test sites were chosen to represent different geological regions and levels of remote sensing as well as scale. The following three sites were chosen.

Nahal Revaha Site

The Nahal¹ Revaha site is located in the central-southern Negev of Israel (Figure 4). The site is part of the Be'er-Sheva's

¹nahal = wadi = ephemeral stream



Figure 9. Automatic extraction of lineaments in the Santa Katharina site. (a) One window. (b) Four windows.

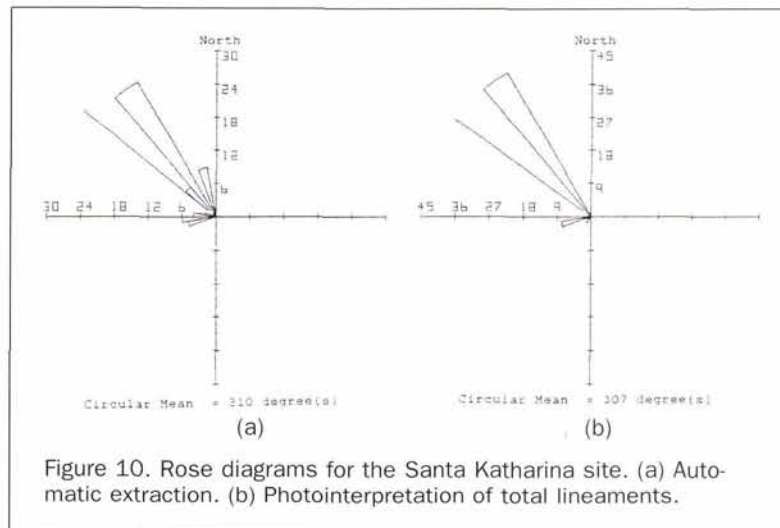


Figure 10. Rose diagrams for the Santa Katharina site. (a) Automatic extraction. (b) Photointerpretation of total lineaments.

basin which is formed by a major syncline west of the Northern Negev Anticlinorium (Arkin *et al.*, 1984). This area is made up of Eocene chalks and limestones covered in some places by Senonian chalk, marl, or chert and younger clastic sediments of Neogene to Quaternary age. A large part of the area is covered by loess, and clear outcrops generally occur only in wadi beds (Figure 5).

This site was chosen as a test site for the evaluation of a hand-held camera photograph taken from the top of an adjacent cliff, approximately 5 m above the test site, representing a "cherry-picker" level of remote sensing (Figure 6). The fracture pattern exposed shows three major trends. In general, the inherent joint pattern trends $N40^{\circ}-50^{\circ}E$ and $S40^{\circ}-50^{\circ}E$. A younger $N60^{\circ}-80^{\circ}E$ trend cuts across all others. These fractures were measured at the test site as well as interpreted

from the photograph. In both cases, the data were evaluated using the stereographic computer program SPLOT by Darton Software.

Computer extracted lineaments are shown in Figure 7. In this case, it is demonstrated that the automatic extraction detects only the major lineaments (Figure 7a). Photointerpretation includes both major and short lineaments (Figure 7b). The automatic extraction process can control the number of lineaments to be counted in each case, thus allowing comparisons to be made at the same level of detection. Figures 8a and 8b represent rose diagrams of lineaments at the same detection level (i.e., the same number of lineaments). It can be seen that the photointerpretation is biased towards the shorter lineaments (Figure 8b) whereas only the major lineaments are detected by automatic extraction (Figure 8a).

When all the lineaments are considered, there is a stronger bias towards the shorter ones (Figure 8c) and the circular mean is rotated clockwise as compared to the ground truth (Figure 7b).

Santa Katharina Site

The Santa Katharina site is located in the central southern Sinai Peninsula (Figure 4). The area is made up of the Katharina-Iqna Pluton which consists of alkaline and older calc-alkaline granitic rocks of Precambrian age (Bentor and Eyal, 1987). The fracture pattern is clearly expressed by the main wadis and dikes cutting across the pluton. The wadis follow the main faults in the area and generally trend north-south. The associated fractures are expressed as both negative and positive dikes as well as clearly defined traces trending $N145^{\circ}E$, $N85^{\circ}E$, $N170^{\circ}E$, and $N37^{\circ}E$ (Figure 1). On this basis, the site was chosen as a test site for low altitude aerial photography evaluation.

Fractures were mapped on vertical air photographs at a scale of approximately 1:10,000 and by automatic extraction (Figure 9; compare with Figure 1). Figures 9a and 9b show the relationship between extracted lineaments from a whole photograph as compared to the extracted lineaments from the same photograph divided into windows. In this case, four windows were chosen; however, there is no limit to the number of windows. The greater the number of windows, the shorter the lineaments that can be detected. These short lineaments merge as windows, are joined adjacently, and they attach end-on, or overlap the longer ones, to form the major lineaments (Figure 9b).

The measured trends were evaluated using SPLOT. Rose diagrams of pole trends of fractures representing total lineaments mapped as compared to the rose diagram of fractures evaluated by automatic extraction are shown in Figure 10. A comparison of rose diagrams of automatic extraction (Figure 10a) and photointerpretation (Figure 10b) shows an obvious agreement between the same level of detection. The circular mean in this case forms a good means for correlation.

Nahal Ye'elim Site

The Nahal Ye'elim site is located on the western side of the Dead Sea Rift Valley (Figure 4). The rocks exposed include Upper Cretaceous Judea Group carbonates and Senonian Mt. Scopus Group chalk and chert (Arkin, 1989). The fractures in the area are representative of the fracture pattern along the length of the rift and are recognized as follows: faults forming the major horsts and grabens along the rift trending in general, $N30^{\circ}W$; the inherent joint pattern representing part of the Dead Sea stress system trending $S45^{\circ}E$ and $N40^{\circ}E$; and secondary fractures trending approximately $N70^{\circ}E$ and $N30^{\circ}E$. A younger fracture system trending $N20^{\circ}E$ and $S8^{\circ}E$ cuts across all others (Arkin, 1989).

This site was chosen as a test site for evaluating fractures on satellite imagery (Figure 11). An automatic extraction of lineament data in the present study, based on Landsat TM, is shown in Figure 12. Figure 13 shows an earlier work of visual lineaments interpretation from Landsat MSS imagery (Arkin and Bartov, 1976). It can be seen that the automatic extraction and photointerpretation at the level of satellite imagery generally allow the detection of major lineaments. Photointerpretation, as shown in Figure 13 at the Nahal Ye'elim site, presents an overall picture of lineaments which are overlapping mapped geological features. These may be compared to that of automated extraction (Figure 12). North is towards the top of Figure 12. It can be seen that the north-south detected lineaments compare well with the general direction of the Dead Sea rift. Other lineaments also set with the directions of major fault lines.

Conclusions

- For the detection of geological lineaments on aerial photographs, which tend to be very bright or very dark, a new variation of the Hough counter has been used. The new counter counts grey levels and operates on both a picture and its inverse, merging the results of line/peak detection.
- The use of the Hough algorithm in the present form allows the automatic detection of most major lineament directions.
- The structure of the present program, by which azimuth and coordinates of lineaments are extracted, allows the mapping of the detected lineaments and their statistical evaluation.



Figure 11. Landsat TM imagery of the Dead Sea area.

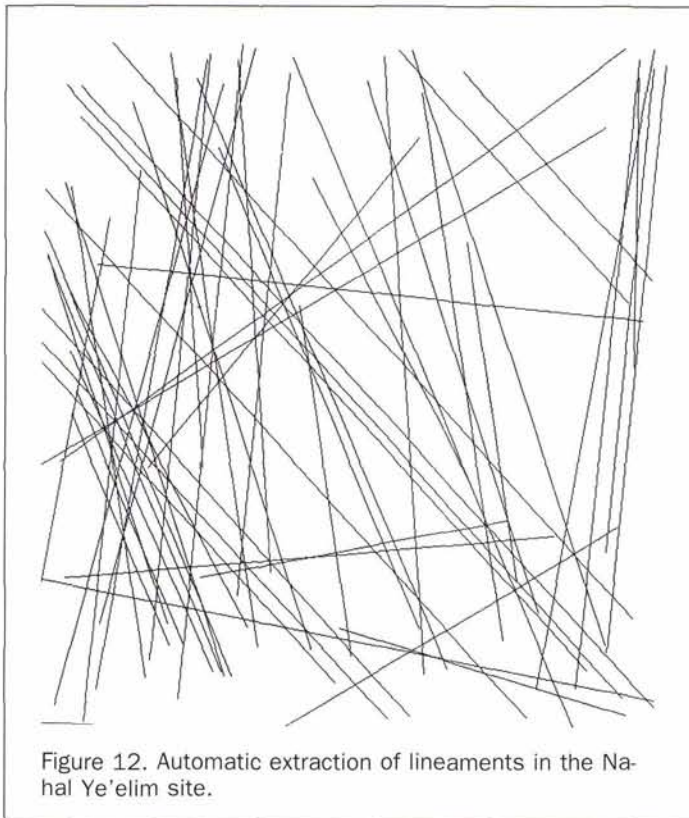


Figure 12. Automatic extraction of lineaments in the Nahal Ye'elim site.

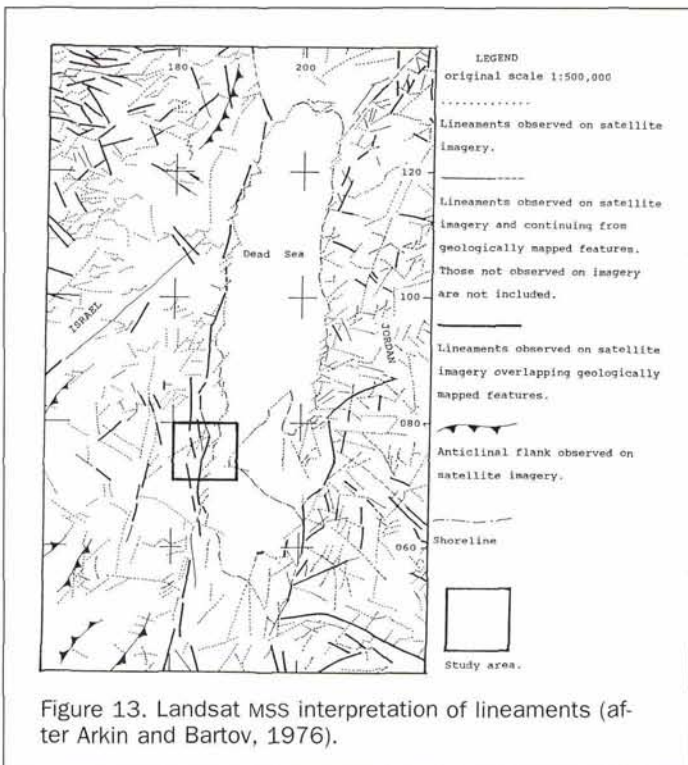


Figure 13. Landsat MSS interpretation of lineaments (after Arkin and Bartov, 1976).

- The option of dividing imagery into windows allows the detection of shorter lineaments in addition to the major ones. This enables the analysis of the minor linear features within the same study area.
- In all three study sites, representing different geological environments, ground truth is seen to be evident by overlapping of automatically extracted lineament directions with known geological features.
- The proposed method of windows applied to satellite digital data could provide more details on geological structures through remote sensing.
- The Hough algorithm may be improved for use on aerial photographs by implementing a large-neighborhood line detector instead of the standard small-neighborhood edge detector.

References

- Arkin, Y., 1989. Large-scale tension features along the Dead Sea — Jordan Rift Valley. *Tectonophysics*, 165:143-154.
- Arkin, Y., and Y. Bartov, 1976. *Lineament Map of Israel Observed on Satellite Imagery*, Isr. Geol. Surv. Rep. MM/5/76, Jerusalem.
- Arkin, Y., Y. Bartov, Z.B. Begin, Y. Druckman, Z. Lewy, Y. Mimran, G. Steinitz, T. Wusbord, and E. Zilberman, 1984. *Outlines of the geology of the northwestern Negev*, Isr. Geol. Surv. Rep. GSI/19/84 (Z.B. Begin, editor), 108 p.
- Ballard, D., and C. Brown, 1982. *Computer Vision*, Prentice-Hall Inc., New York.
- Bartov, Y., and M. Eyal, 1987. *The Geology of Southern Sinai, Its Implication for the Evaluation of the Arabo-Nubian Massif*, Israel Academy of Science and Humanities, Jerusalem.
- Cross, A., 1988. Detection of circular geological features using the Hough transform, *Int. J. Remote Sensing*, 9:1519-1528.
- Cross, A., and G. Wadge, 1988. Geological lineaments detection using the Hough transform, *IGARSS'88 Proceedings*, pp. 1779-1782.
- Oakes, G., 1987. *Automatic Lineament Analysis Techniques for Remotely Sensed Imagery*, Ph.D. Thesis, Imperial College, University of London.
- Rowan, L.C., and E.H. Lathram, 1980. Mineral exploration, Chapter 17 in *Remote Sensing in Geology* (B.S. Siegal and A.R. Gillespie, editors), John Wiley & Sons, New York, pp. 553-605.
- Rosenfeld, A., J. Ornelas, and Y. Hung, 1986. *Hough Transform Algorithms for MESH-Connected SIMD Parallel Processors*. University of Maryland, Center for Automation Research, CAR-TR-178, February.
- Sijmons, K., 1987. Computer-assisted detection of linear features from digital remote sensing data, *ITC J.*, 1987-1:23-31.
- Simon, B., R. Jacquier, P.H. Oltra, and M. Popoff, 1989. Detection automatique des structures orientées du fosse de la Benoue (Nord-Est Nigeria), *Bull. Société Française de Photogrammétrie et de Télédétection*, No. 115.
- Tibaldi, A., and L. Ferrari, 1991. Multisource remotely sensed data, field checks and seismicity for the definition of active tectonics in Ecuadorian Andes, *Int. J. Remote Sensing*, 12:2344-2358.
- Wang, J., and P.J. Howarth, 1989. Edge following as graph searching and Hough transform algorithms for lineament detection, *IGARSS'89 Proceedings*, pp. 93-96.
- , 1990. Use of the Hough transform in automatic lineament detection, *IEEE Transaction on Geoscience and Remote Sensing*, 28:561-566.
- Waters, P., 1990. Methodology of lineament analysis for hydrogeological investigations. Chapter 11 in *Satellite Remote Sensing for Hydrology and Water Management* (E.C. Barret, C.H. Power, and A. Micallef, editors), Gordon and Breach Science Publications, New York, pp. 197-214.
- Zlatopolsky, A.A., 1992. Program LESSA (Lineament Extraction and Stripe Statistical Analysis) Automatic Linear Image Features Analysis — Experimental Results, *Computer and Geosciences*, 18:1121-1126.

(Received 31 March 1993; revised and accepted 2 December 1993; revised 10 May 1994)